Matter

CellPress

Article

Microbially driven reversible size- and color-changing materials

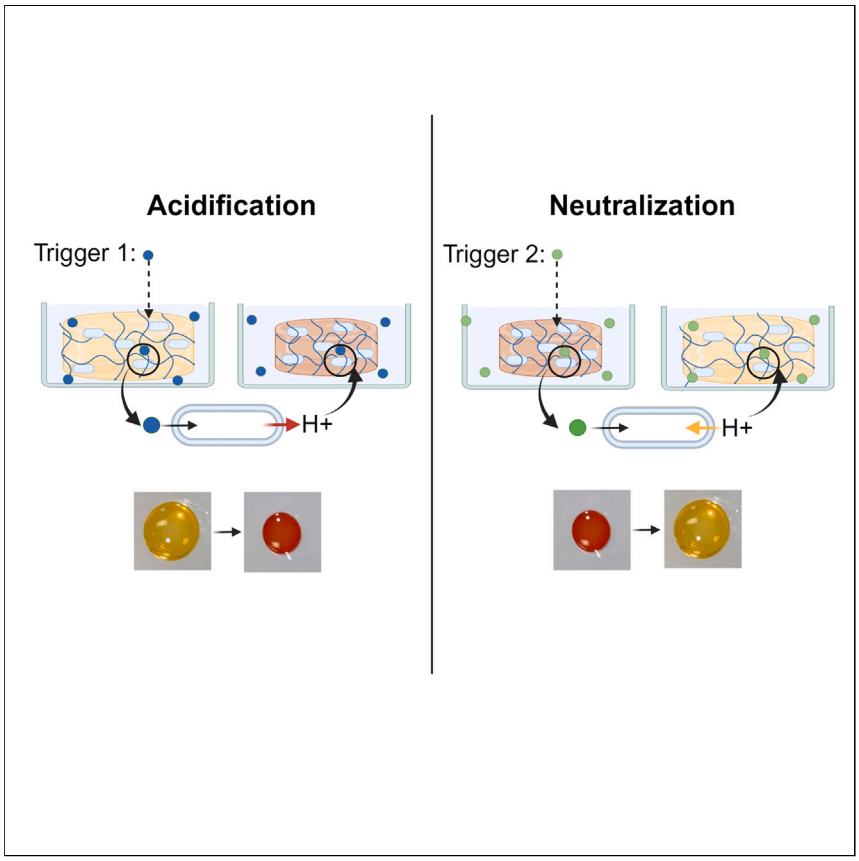

A challenge of engineered living materials is employing living components to drive changes in their environment. This work demonstrates the alteration of pH driven by *Escherichia coli*, resulting in reversible size and color change of a pH-responsive hydrogel. This validates a new concept with potential applications in more sophisticated hydrogel-based shape-changing materials.

Jenevieve Kuang, Shanna Bonanno, Wei-Ting Chang, ..., Daniel J. Wilson, Leila F. Deravi, Neel S. Joshi

ne.joshi@northeastern.edu

Highlights

E. coli alters pH with varied carbon sources in a reversible and predictable manner

E. coli enables changes in size and color of a pH-responsive hydrogel

The living material displays reversible appearance changes inspired by nature

4 **Demonstrate**
Proof-of-concept of performance with intended application/response

Kuang et al., Matter 7, 1–19
May 1, 2024
https://doi.org/10.1016/j.matt.2024.03.009

Please cite this article in press as: Kuang et al., Microbially driven reversible size- and color-changing materials, Matter (2024), https://doi.org/10.1016/j.matt.2024.03.009

Matter

CellPress

Article

Microbially driven reversible size- and color-changing materials

Jenevieve Kuang,[1,8] Shanna Bonanno,[2,8] Wei-Ting Chang,[1] Duncan Q. Bower,[1] Violet M. Pratt,[1,2] Jillian Zerkowski,[1] Nicholas Scaperdas,[2] Lindsey A. Young,[3] Olivia J. Armendarez,[1] Mohammed H. Alwelyee,[4] Samantha L. Lim,[5] Daniel J. Wilson,[6,7] Leila F. Deravi,[1] and Neel S. Joshi[1,2,9,*]

SUMMARY

Features of natural living systems underexplored in engineered living materials (ELMs) are macroscale appearance changes driven by active cellular processes. To overcome this technological gap, we demonstrate an ELM wherein the natural metabolism of *Escherichia coli* is used to drive reversible changes in pH-responsive hydrogels through the production or consumption of acidic metabolites. A color-changing function of the hydrogels relies on the custom design, synthesis, and coupling of a synthetic pH indicator dye into the polymer network. Manipulation of the starting pH conditions and the identity of the primary carbon source leads *E. coli* to alter pH, resulting in reversible size and color changes in the gels. Arrayed arrangements of multiple responsive hydrogels can mimic dynamic pixels that respond to changes in cell metabolism. Here, we expand the tool kit of ELMs to include size and color change as functional performance features that can be driven by active cellular processes.

INTRODUCTION

Natural systems, from unicellular organisms to mammals, employ unique actuation mechanisms using their own tissues for many adaptation and survival behaviors, ranging from locomotion to reproduction. For example, bacterial flagella function as molecular motors driven by ATP hydrolysis[1]; plants have evolved seed pods that open in response to favorable growth conditions or move to disseminate progeny to other locations[2]; the musculoskeletal system of animals enables transportation and agility.[3] Color modulation is another phylogenetically widespread and mechanistically diverse evolutionary adaptation. Cyanobacteria change their color to optimize light absorption depending on their environment[4]; trees change the color of their leaves for metabolic conservation.[5] Remarkably, cephalopods combine mechanical actuation of their tissues with color change to perform changes in visual appearance.[6] In most of these examples, living cells play a crucial role in converting chemical fuel into various forms of molecular motion and pigmentary changes.

The emerging field of ELMs combines cells and materials in ways that seek to recapitulate some of the alluring dynamism of natural living systems. Examples of ELMs include systems in which either the cells, the material, or both are engineered to achieve particular performance characteristics. ELMs have harnessed the unique ability of cells to perform biochemical and environmental sense-and-respond functions. Examples include wearable elastomeric devices containing cells that fluoresce

PROGRESS AND POTENTIAL

Engineered living materials (ELMs) integrate cells and materials with the goal of recapitulating the dynamics of living systems in nature but with more controllable elements. Nevertheless, mimicking macroscale appearance changes of natural systems enacted by active cellular processes remains a challenge. Here, we develop an ELM composed of a pH-responsive hydrogel embedded with *Escherichia coli*. pH modulation driven by the central metabolism of the living component triggers reversible changes in the size and color of the hydrogel matrix. This work shows a proof-of-concept of an engineered living system that undergoes prescribed appearance changes based on a combination of materials and cellular engineering. It may potentially enhance the dynamic performance of other conventional materials and ELMs that have been used in drug delivery, hydrogel origami, and soft robotics applications.

Please cite this article in press as: Kuang et al., Microbially driven reversible size- and color-changing materials, Matter (2024), https://doi.org/10.1016/j.matt.2024.03.009

in response to chemical cues,[7] ingestible bacterial-electronic systems for sensing blood in the gut,[8] and yeast-based cellulose materials for detecting hormone pollutants in water.[9] Other ELM efforts have leveraged the ability of cells to produce new materials and structures, as in the case of concrete that heals itself with microbially induced carbonate precipitation,[10] and bacterial cellulose fabricated in 3D molds with self-healing capabilities.[11]

ELMs with several other intriguing functions exist, but cell-driven mechanical actuation and color change remain underexplored. In one of the few existing examples of an ELM exhibiting cell-driven mechanical actuation, auxotrophic yeast were embedded into a poly-acrylamide hydrogel. When given the necessary nutrients, yeast cell division led to the swelling of the gel matrix up to four times its original size.[12] Although impressive in terms of size change and cost-effectiveness, the process is inherently irreversible because it relies on cell division as the actuation mechanism. Another example that uses bacterial spores involved in mechanical actuation includes the deposition of microbial cells on a humidity-inert material where hydration and dehydration lead the cells to modulate the shape of a biohybrid composite.[13] While this example shows reversible actuation, it is not governed by active cellular processes, but rather the hygroscopic behavior of the spores. A specialized example involved the use of mammalian cardiomyocytes seeded onto flexible PDMS films with patterned lines of fibronectin. In the presence of appropriate nutrients, the cells apply coordinated periodic contractile forces to bend the PDMS films. Through the clever application of geometric constraints, the cell-elastomer composite exhibited swimming behavior, akin to an artificial jellyfish.[14] However, the implementation of this system is hindered by the onerous nutrient requirements for mammalian cells and their sensitivity to contamination.

We sought an alternative approach to simultaneous cell-driven actuation and color change based on the well-known phenomena of pH-responsive hydrogels.[15] Polyionic hydrogels bearing appropriate electrostatically charged functional groups can undergo reversible size change if those functional groups change their charge state at different pH values. For example, the carboxylate groups of mannuronate and guluronate in alginate have pK_a values of 3.4 and 3.7, respectively.[16] At pH values above the pK_a, the carboxylate group is deprotonated and negatively charged, leading to swelling of the gel. At pH values below the pK_a, the protonation of the carboxylate group decreases water solubility and drives out water by comparison, de-swelling the gel. This general principle has been used for drug delivery,[17] hydrogel origami,[18] and soft robotics,[19] among other applications. A limitation of pH-responsive hydrogels is that the pH change must come from an external source—a mechanism that limits practical deployment. Instead, we demonstrate a system wherein the pH change is driven by living cells within and surrounding the gel. Research has been conducted on the confinement of microbes to a hydrogel matrix for specific deployable systems, where the matrix is designed to support cell growth.[7,20,21] However, due to the dynamic swelling behavior of pH-responsive hydrogels, we designed our system to act as a repository for populating the surrounding medium with *E. coli* during each half cycle after medium changes.

E. coli is known to alter the pH of its surroundings depending on the identity of the primary carbon source.[22] For example, in the presence of excess glucose and with oxygen as the limiting nutrient, *E. coli* metabolism generates acidic fermentation byproducts, such as lactic and acetic acids.[22,23] Conversely, if *E. coli* is supplied with acidic starting conditions, it can consume acids, neutralizing its environment.[22,23] Like most living organisms, *E. coli* prefer to be at neutral pH, and have capabilities

[1]Department of Chemistry and Chemical Biology, Northeastern University, Boston, MA 02115, USA

[2]Department of Bioengineering, Northeastern University, Boston, MA 02115, USA

[3]Department of Mechanical and Industrial Engineering, Northeastern University, Boston, MA 02115, USA

[4]Department of Biomedical Engineering, Boston University, Boston, MA 02215, USA

[5]Department of Computer Science, Rice University Houston, Houston, TX 77005, USA

[6]Kostas Research Institute, Northeastern University, Burlington, MA 01803, USA

[7]Department of Chemical Engineering, Northeastern University, Boston, MA 02115, USA

[8]These authors contributed equally

[9]Lead contact

*Correspondence: ne.joshi@northeastern.edu

https://doi.org/10.1016/j.matt.2024.03.009

Please cite this article in press as: Kuang et al., Microbially driven reversible size- and color-changing materials, Matter (2024), https://doi.org/10.1016/j.matt.2024.03.009

to increase pH to achieve homeostasis when exposed to acidic conditions. These mechanisms include controlling the direction of proton flux across the cell membrane, shifting metabolic pathways to reduce the production of acidic byproducts, and producing enzymes that catalyze the formation of weak bases.

Here, we demonstrate the use of *E. coli*'s pH modulation capabilities to drive reversible swelling and color change in a synthetic material (Figures 1A and 1B). Given the dearth of biomolecular machinery in *E. coli* capable of directly applying mechanical force to its surroundings, akin to the actin-myosin and cytoskeletal machinery in eukaryotic systems, we use pH as a mediator between cells and the material. Nevertheless, the fusion of tailored synthetic material properties and cellular metabolic capabilities is inspired by natural living systems that have achieved this union through evolution.

RESULTS AND DISCUSSION

Principle and design of microbially driven display

After screening several candidate hydrogel compositions, we selected poly(acrylamide-co-acrylic acid), or "PAAcAAm," because of its biocompatibility, ease of fabrication, mechanical robustness, and reversible swelling behavior between pH 4.0 and 7.0—a range compatible with *E. coli* survival. We also sought to incorporate a pH-responsive dye into the hydrogel matrix to achieve color and size change simultaneously. We wanted a dye that could provide visible color changes in a pH range accessible by *E. coli*. Methyl red seemed like an ideal candidate based on these constraints. Preliminary experiments revealed that simple encapsulation would be insufficient for our purposes, since the dye leached during reversible swelling cycles, hindering precise visualization of gel size. To prevent this, we sought to incorporate the dye covalently into the hydrogel polymer matrix. Literature precedent suggested that the most straightforward functionalization strategy—amide bond formation at the methyl red carboxylate—would change the halochromic behavior of the dye.[24] Therefore, we designed and synthesized the derivative MR-2, which preserves the zwitterionic structure of methyl red (and its color change at pH 4.5) while allowing for covalent incorporation into the hydrogel matrix during polymerization. The two-step synthesis of MR-2 began with a diazonium coupling between anthranilic acid and 1-phenylpiperazine to produce azo compound MR-1 in 40% yield. This was followed by a reaction with acryloyl chloride to produce MR-2 in 60% yield after column purification (Figure 2A).

Functional validation of size- and color-changing hydrogel

Following the concentrations of gel components as described in the experimental procedures (Table 1), we fabricated hydrogels by co-polymerizing acrylic acid, acrylamide, and MR-2 in the presence of a crosslinker (Figure 2B). Polymerizations were performed by combining 60 μL of precursor, initiator, and catalyst in 3D-printed resin molds to achieve cylindrical hydrogels with a diameter of 6 mm and a height of approximately 2 mm. These hydrogel "pucks" were tested for their size and color changing abilities by immersion in aqueous buffers at various pH values (Figures 2C–2H). Pucks equilibrated at pH 7.0 were swollen and exhibited the characteristic yellow color of methyl red, while those equilibrated at pH 4.0 were smaller and red in color (Figure 2C). Higher loading of the MR-2 dye yielded pucks with more vibrant colors, although the maximum dye loading was limited by MR-2 solubility in the pre-polymerization solution. We subjected the pucks with various MR-2 loading densities to alternating cycles of equilibration, first in pH 7.0, and then in pH 4.0 aqueous buffer. The average cross-sectional surface area of the hydrogel pucks increased from 28 mm^2 directly after polymerization to 76 mm^2 after initial pH 7 equilibration.

Please cite this article in press as: Kuang et al., Microbially driven reversible size- and color-changing materials, Matter (2024), https://doi.org/10.1016/j.matt.2024.03.009

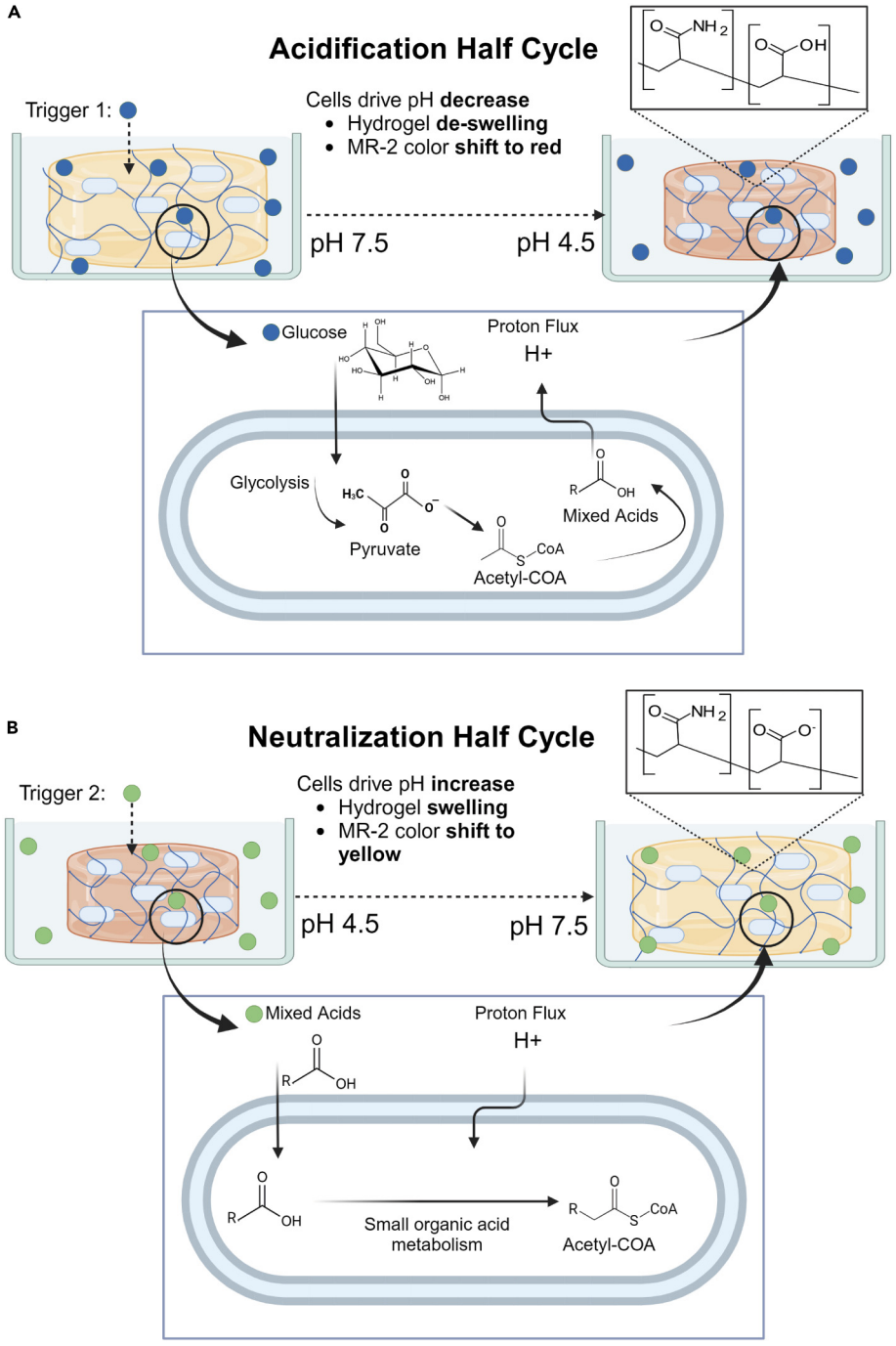

Figure 1. Engineered size- and color-changing living material

Schematic of engineered microbially driven hydrogel size and color change.

(A) In the presence of excess glucose, *E. coli* produces acidic byproducts, lowering the pH of its surroundings. This leads to hydrogel de-swelling and a color change from yellow to red.

(B) In the absence of glucose, and at a starting pH of 4.5, *E. coli* consumes acidic metabolites, raising the pH of its surroundings. This leads to hydrogel swelling and color change from red to yellow.

Next, their average cross-sectional area decreased to 40 mm^2 under acidic conditions (a ~50% decrease from the equilibrated hydrogel pucks) and increased back to 74 mm^2 under basic conditions reversibly over two full cycles for all MR-2 loading

Please cite this article in press as: Kuang et al., Microbially driven reversible size- and color-changing materials, Matter (2024), https://doi.org/10.1016/j.matt.2024.03.009

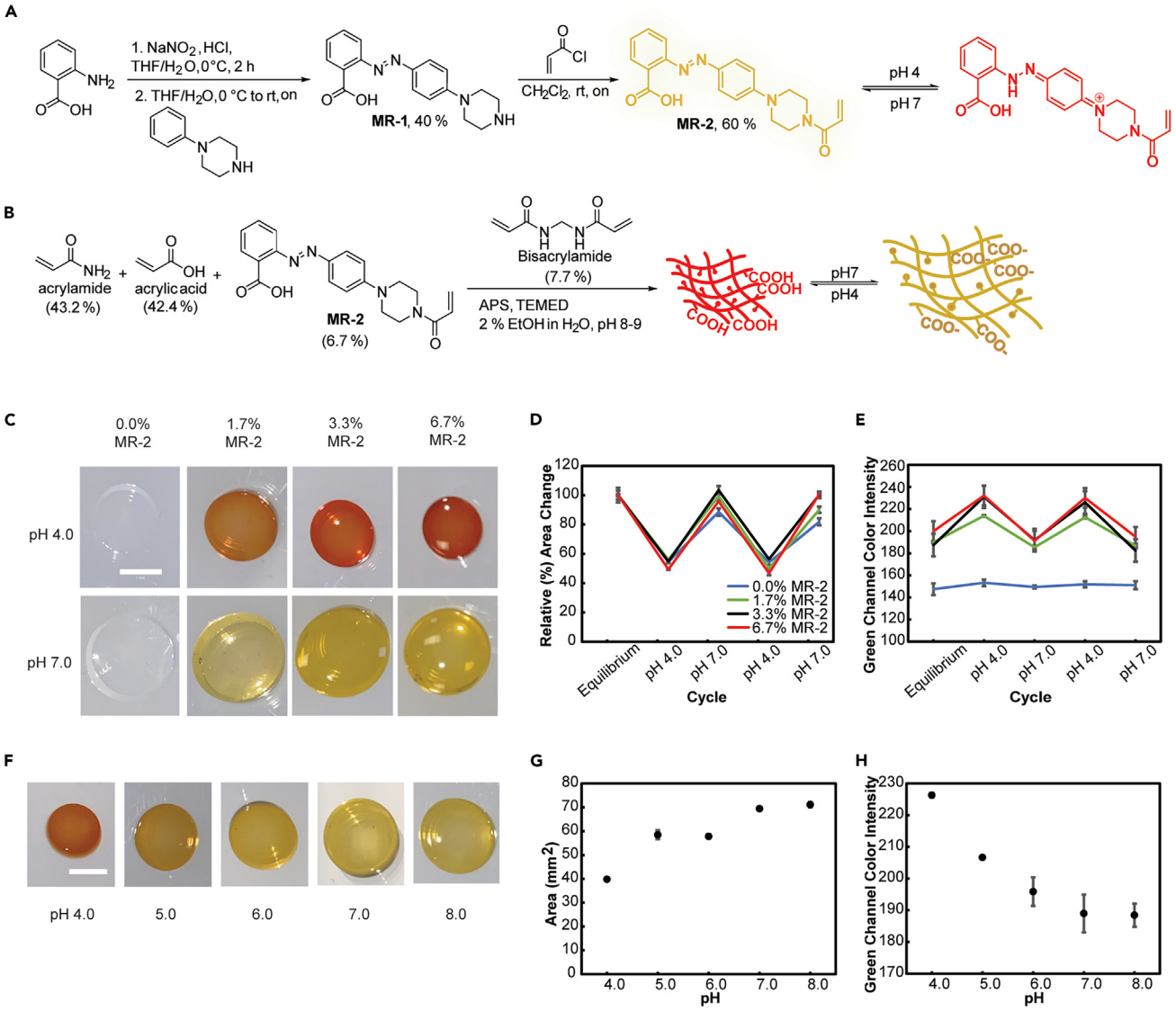

Figure 2. MR-2 hydrogel fabrication and characterization

(A) Scheme for MR-2 synthesis and schematic of its pH-induced color change.

(B) Synthetic scheme for MR-2-loaded PAAcAAm hydrogel formation.

(C) Representative images of hydrogel pucks at various MR-2 loading densities (0%, 1.7%, 3.3%, and 6.7% [w/v] relative to total monomer molarity) after equilibration in pH 4.0 sodium citrate buffer (top) and pH 7.0 Tris buffer (bottom).

(D and E) Relative hydrogel cross-sectional area measurements (D) and green channel intensity analysis (E) of hydrogel pucks (n = 3) after equilibration in pH 4.0 and pH 7.0 buffers over two full cycles.

(F) Representative images of 6.7% MR-2 hydrogel pucks equilibrated at various intermediary pH values.

(G and H) Relative hydrogel cross-sectional area measurements (G) and green channel intensity analysis (H) of 6.7% MR-2 hydrogel pucks (n = 3) after equilibration in buffers at various intermediary pH values. Data in (D), (E), (G), and (H) are represented as mean ± SD. Scale bars, 5 mm. NMR spectra for MR-1 and MR-2 are represented in Figures S1–S4.

densities (Figure 2D). We also evaluated puck color by the RGB color model. When looking at the contributions of each channel (red, green, and blue) at different pH values, we found the largest MR-2 color changes in the green channel, representing pixels at the central wavelength of 550 nm.[25] Therefore, we measured and reported puck color change based on a pixel intensity value (ranging from 0 to 255) in the green channel. We observed similar cycles of increase and decrease in green channel intensity after pH equilibration for all loading densities compared with the 0%

Please cite this article in press as: Kuang et al., Microbially driven reversible size- and color-changing materials, Matter (2024), https://doi.org/10.1016/j.matt.2024.03.009

Table 1. Final concentrations of precursor gel components before polymerization

AA:Aam[a]	AA:Bis[b]	Bis:MR-2[c]	Bis:ammonium persulfate[d]	Bis:TEMED[e]
1:1.02	1:0.06	1:2.83	1:2.03	1:0.68

[a]The molar ratio of acrylic acid to acrylamide.
[b]The molar ratio of acrylic acid to bis-acrylamide crosslinker.
[c]The molar ratio of bis-acrylamide crosslinker to MR-2.
[d]The molar ratio of bis-acrylamide crosslinker to ammonium persulfate.
[e]The molar ratio of bis-acrylamide crosslinker to TEMED.

MR-2 control (Figure 2E). The 6.7% MR2 composition was selected for all experiments conducted moving forward. Finally, we measured the color and shape change at intermediary pH values (Figures 2F–2H), confirming larger changes in both parameters closer to the predicted pK_a of MR-2 (pK_a = 5.1) and acrylic acid (pK_a = 4.2).

Dynamic color changing in perfusion chamber

To test the longevity of the material system and facilitate the collection of time-resolved data, we constructed a custom perfusion chamber (made of polymethyl methacrylate, PMMA) capable of automated switching between two input reservoirs (Figures 3A and S5). Seven hydrogel pucks were placed inside the perfusion chamber, held in place by a 3D-printed insert. The chamber was sealed to prevent the leaking of fluid and to ensure that the hydrogels remained fully immersed in the aqueous buffer. This device enabled automated fluid exchanges to cycle between neutral and acidic pH conditions. Puck size and color were tracked continuously over the course of 2 weeks by placing the chamber in the bed of a photo scanner programmed to collect scans of the hydrogel pucks every 10 min. Using a microcontroller (Arduino Uno), we programmed the flow of aqueous buffers, alternating between pH 4.0 sodium citrate and pH 7.0 Tris buffer every 12 h, with stopped flow in between. The volume of the perfusion chamber was approximately 20 mL. Buffer exchanges were maintained at a constant rate (7.5 mL/min) until 25 chamber volumes of buffer had passed through the perfusion chamber (approximately 500 mL). The goal of the buffer exchange was to allow for adequate clearance of the previous buffer before allowing the hydrogel pucks to equilibrate in the next buffer. The pucks changed size and color as expected, requiring approximately 10 h to reach equilibrium, as represented by the images for one acidification half cycle in pH 4.0 sodium citrate buffer (Figure 3B). The puck size and color intensity switching behavior were robust throughout the entire 2-week experiment (Figures 3C and 3D). Due to fluid leaking during the first 50 h of the experiment, data plotted starts at 50 h when accurate cycling began. Further evidence of size and color change can be found in Video S1.

Encapsulation and viability of *E. coli* in PAAcAAm hydrogels

To track bacteria after encapsulation inside the MR-2 loaded PAAcAAm hydrogels, we first transformed *E. coli* (BL21) with a plasmid encoding green fluorescent protein (GFP) under the control of an inducible promoter. Encapsulation proceeded by resuspending pelleted bacteria (2.3×10^{10} CFU) in 1 mL of the hydrogel precursor solution, followed by polymerization inside the resin mold to achieve 60 μL cylindrical pucks with a height of 2.1 mm and a diameter of 6.0 mm (Figure 4A). The approximate cell density per individual hydrogel puck was 1.4×10^9 CFU. The cell-hydrogel composites were initially equilibrated in pH 7.5 Luria-Bertani (LB) medium at 37°C overnight. Confocal microscopy revealed an even distribution of bacteria within the gel, aside from the non-uniformity at the bottom of the 3D rendering. Cell settling during the 1-h static (non-agitated) polymerization conditions of the cell embedded hydrogel could be a possibility for this non-uniformity (Figure 4B). The stability of the

Please cite this article in press as: Kuang et al., Microbially driven reversible size- and color-changing materials, Matter (2024), https://doi.org/10.1016/j.matt.2024.03.009

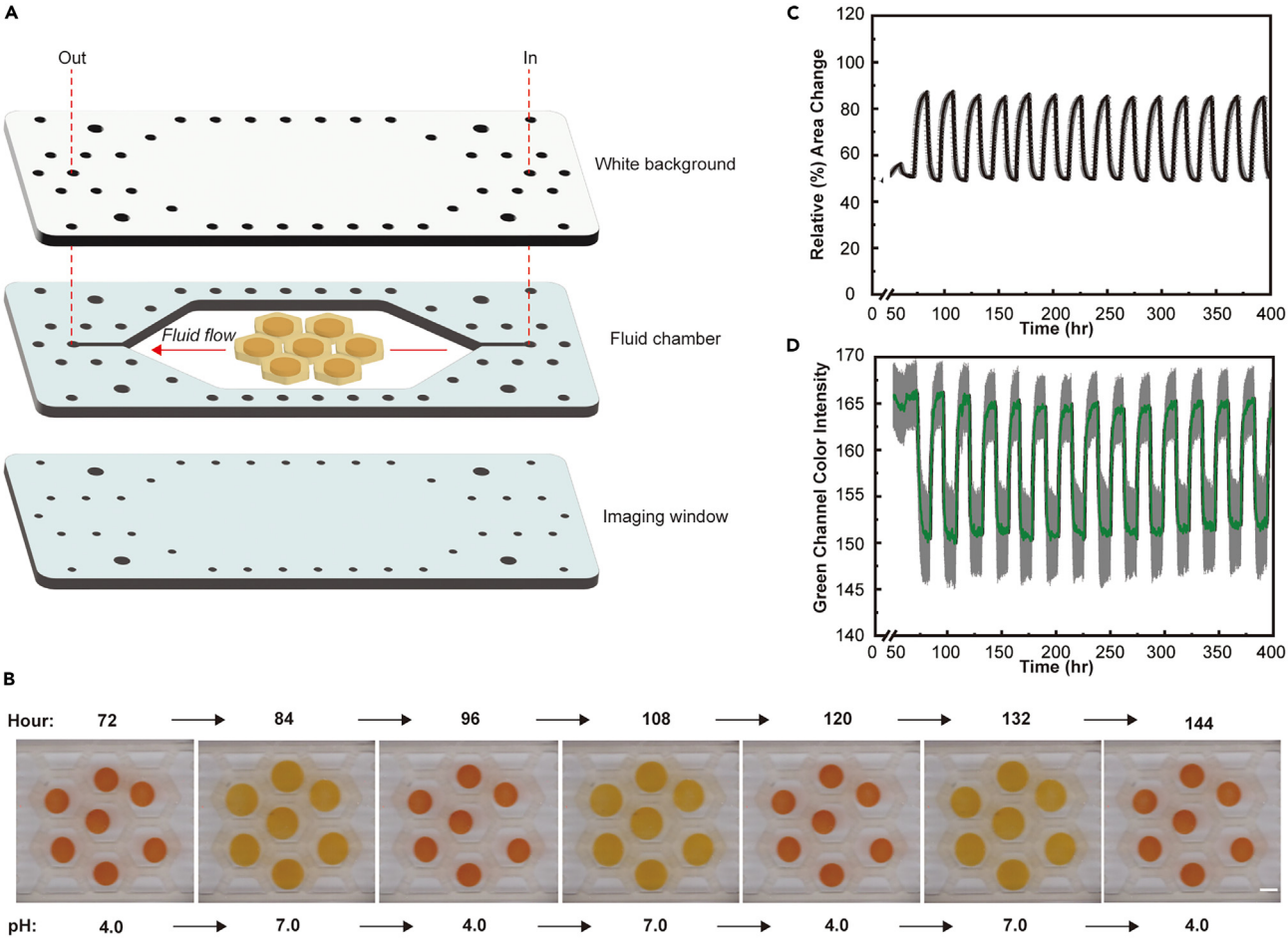

Figure 3. Tracking cell-free hydrogel size and color changes in an automated perfusion chamber

(A) Exploded schematic of the perfusion chamber housing seven MR-2 containing hydrogels in line with fluid flow.

(B) Representative images of hydrogels inside the perfusion chamber over the course of three full cycles. Scale bar, 5 mm.

(C and D) Automated continuous tracking of hydrogel cross-sectional area (C) and green channel intensity (D) of hydrogels (n = 7) over the course of 2 weeks of cycling between pH 4.0 and pH 7.0 aqueous buffer. The flow was stopped between buffer switches. In (C), 100% indicates cross-sectional area immediately after equilibration in pH 7.0 buffer, post-polymerization. Data are represented as mean ± SD (shaded in gray). Across 14 full cycles the average standard deviation was 0.02 (%) and 3.93 (green channel value) for size change and color change, respectively.

PAAcAAm matrix precluded the recovery of viable bacteria for cell counting after encapsulation. We tried other dye-based commercial kits for monitoring cell viability (e.g., BacTiter-Glo), but these were not effective for quantitative measurements (Figure S6), possibly because of mass transport limitations hindering dye diffusion into the gel. In addition, we tried to calculate cell viability from the confocal images. This calculation yielded 1.4×10^7 CFU per puck, which was conducted by counting cells in a bisected slice of one hydrogel puck using leaky cytosolic GFP to track each cell. The cell density was extrapolated to an entire hydrogel puck. Because leaky GFP expression cannot be directly correlated to the viability of cells when images were taken, and induction of GFP was not possible due to saturated signal, this is a mere approximation of cell viability. Therefore, to obtain a qualitative understanding of cell viability after polymerization, we encapsulated uninduced *E. coli* and immersed the pucks in a growth medium with the inducer. We observed clearly higher fluorescence signal in these gels compared with control experiments without any inducer or with cells transformed with a sham plasmid (Figure 4C). Some

Please cite this article in press as: Kuang et al., Microbially driven reversible size- and color-changing materials, Matter (2024), https://doi.org/10.1016/j.matt.2024.03.009

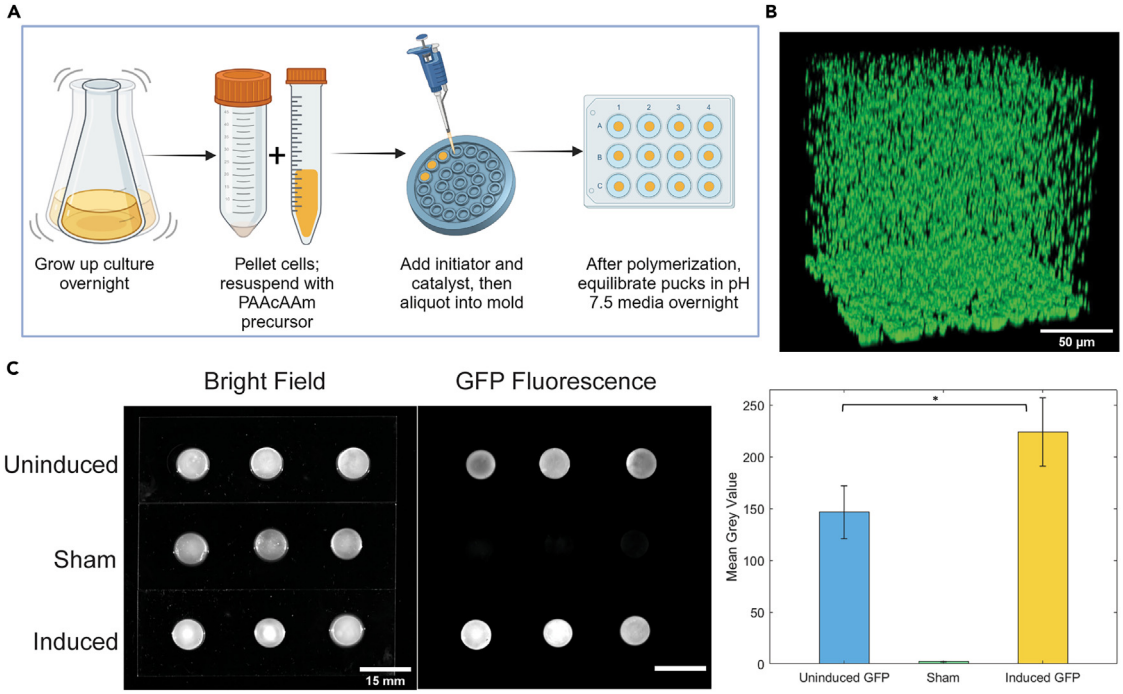

Figure 4. Spatial distribution and viability of *E. coli* in PAAcAAm hydrogels

(A) Workflow for cell encapsulation in PAAcAAm hydrogels.

(B) Reconstructed z stacks of representative hydrogel-encapsulated *E. coli* from confocal microscopy. Green fluorescence signal arises from cellular GFP production and suggests a cell density of 1.4×10^7 CFU in a polymerized PAAcAAm puck.

(C) Hydrogel pucks with cells ($n = 3$) containing inducible genes encoding GFP were imaged in bright-field and fluorescence mode. After polymerization, gels were immersed in growth medium either without (top) or with (bottom) inducer for 24 h. A negative control consisting of gels with cells harboring a sham plasmid (i.e., no GFP gene) was included to account for cell autofluorescence (middle). The mean gray values for the GFP fluorescent image were plotted (right) to compare signal intensity between conditions. A paired t test was used to compare uninduced to induced GFP conditions ($n = 3$, ns, $p > 0.05$, $^*p < 0.05$). Scale bars, 15 mm.

background fluorescence signal was observed in the uninduced control, which we attribute to leaky GFP expression. We ruled out cell autofluorescence based on the difference between sham and uninduced controls. Overall, the enhanced fluorescence signal from cells induced after polymerization suggested that the cells were able to survive the encapsulation process and remain metabolically active.

Microbial modulation of environmental pH, hydrogel swelling, and color

To investigate the ability of *E. coli* (BL21) cells to modulate the pH of their surrounding environment, we grew the bacteria in LB medium supplemented with glucose (2%) at 37°C for 20 h. The pH of the medium decreased from 7.0 to a mean pH of 4.5 over this time while growing from a starting CFU of 8.8×10^8 ($OD_{600} = 1.5$) to 1.79×10^9 CFU ($OD_{600} = 3.06$). In a separate experiment, we supplemented LB medium with acetate (1 mM) and adjusted the pH to 4.5 prior to seeding with the same cell density. After 18 h at 37°C, the endpoint pH was determined to be 8.5 on average with an endpoint cell density of 1.63×10^9 CFU ($OD_{600} = 2.78$) (Figure S7).

We then used this pH-modulating tendency of *E. coli* to drive hydrogel size and color change. First, we encapsulated *E. coli* harboring the sham plasmid in MR-2-containing hydrogels. After fabrication, the hydrogel pucks with or without *E. coli* were allowed to equilibrate in pH 7.5 LB broth with no glucose supplementation for 20 h at 37°C to achieve equilibrium swelling and color states (Figure 5A). During acidification half cycles, the pucks were incubated in LB medium supplemented with

Please cite this article in press as: Kuang et al., Microbially driven reversible size- and color-changing materials, Matter (2024), https://doi.org/10.1016/j.matt.2024.03.009

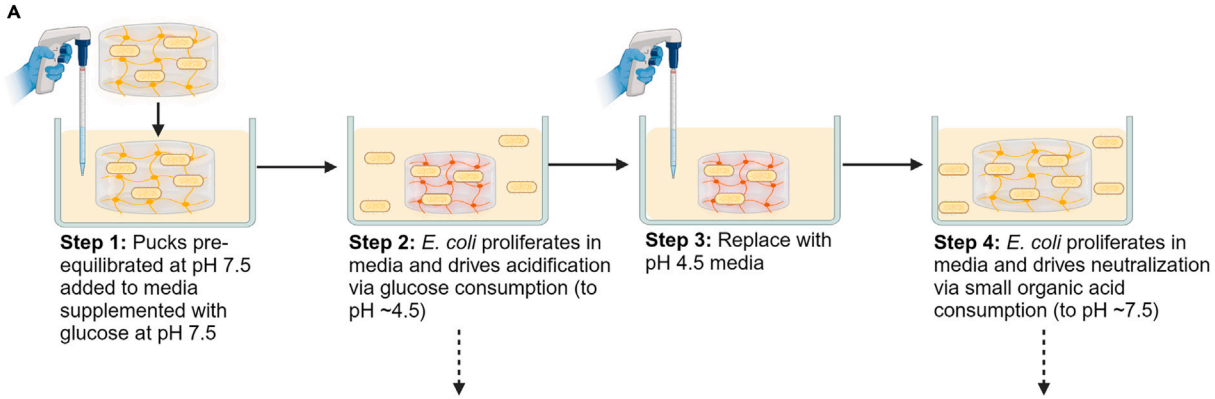

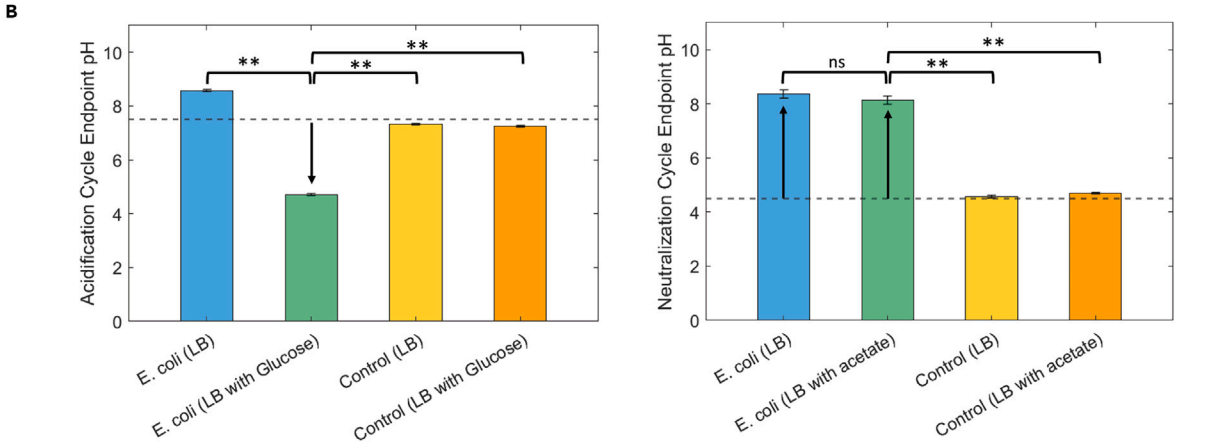

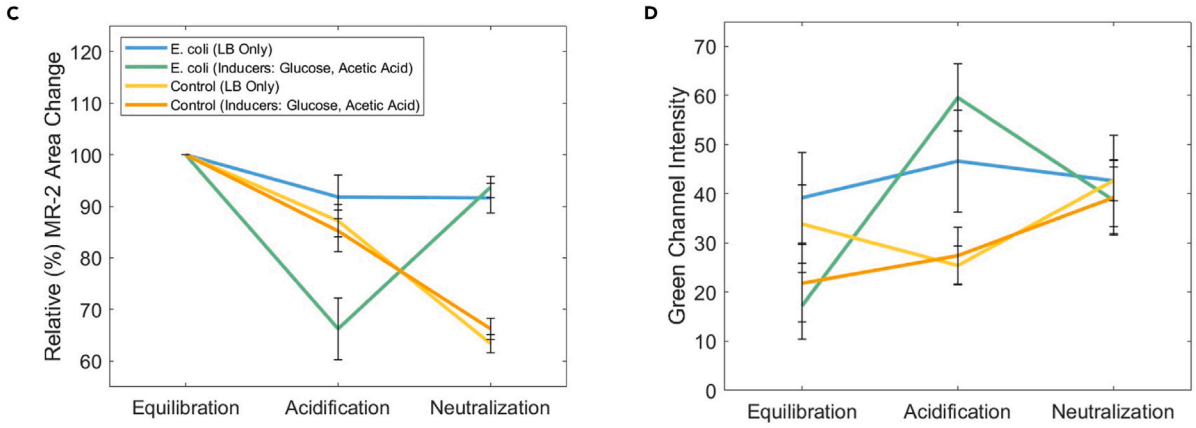

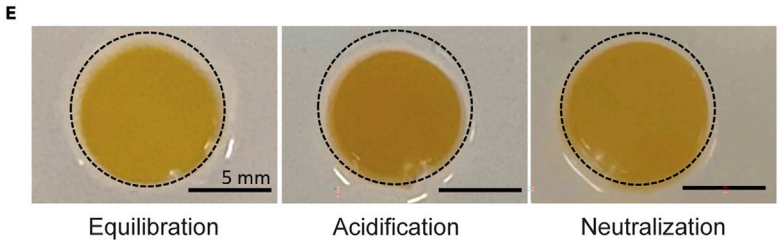

Please cite this article in press as: Kuang et al., Microbially driven reversible size- and color-changing materials, Matter (2024), https://doi.org/10.1016/j.matt.2024.03.009

Figure 5. Cell-driven pH, size, and color change in living hydrogels

(A) Experimental workflow for hydrogel pucks with embedded *E. coli* after fabrication.

(B) Endpoint pH for acidification half cycle (left) and neutralization half cycle (right). The dotted line represents the pH at t = 0 h for a given half cycle.

(C) Hydrogel cross-sectional area measurements at the endpoint of each half cycle. 100% represents the area after the initial equilibration in pH 7.5 growth medium.

(D) Green channel color intensity values for hydrogels at equilibration, acidification, and neutralization endpoints.

(E) Representative images of PAAcAAm-MR-2 hydrogels with embedded *E. coli* at the endpoint of each half cycle. The solid line indicates the area designated as 100%.

One-way ANOVA followed by Tukey's test was used to compare groups at a given half cycle in (C) and (D) ($n = 5$, ns, $p > 0.05$, $^{*}p < 0.05$, $^{**}p < 0.01$). Paired t tests were used to compare half-cycle endpoints within a given group ($n = 5$, ns, $p > 0.05$, $^{*}p < 0.05$). Statistical tests are plotted in Figure S9. Data in (B)–(D) are represented as mean ± SD.

glucose (2%) for 20 h at 37°C. Over the course of the half cycle, the mean pH of the medium decreased to 4.7, while control experiments in the absence of glucose, cells, or both, did not show significant pH change compared with the equilibrated state (Figure 5B, top). The decrease in pH also caused a 30% mean decrease in the cross-sectional surface area of the hydrogels (Figure 5C). The negative control gels did not exhibit a significant change in cross-sectional area. Cell-driven acidification also led to a shift in MR-2 color as demonstrated by the change in green channel intensity from 17.2 ± 6.8 to 59.6 ± 6.9, before and after acidification, respectively (Figure 5D).

For the neutralization half cycle, the pucks were transferred to medium supplemented with acetate (1 mM) whose starting pH had been adjusted to 4.5. We selected acetate supplementation since it is a known carbon source that leads to an increase in pH in the surrounding environment.[22] We included conditions with and without acetate supplementation, like the format of glucose supplementation during the acidification cycle. As expected, pucks that did not contain cells did not alter the pH of their surroundings at all after incubation. However, pucks containing cells were able to raise the pH of the surrounding medium to a mean value of 8.1 (Figure 5B, bottom). Interestingly, we observed neutralization regardless of acetate supplementation. This is likely due to *E. coli*'s ability to consume mixed organic acids that already exist in LB medium. Pucks containing cells re-swelled close to their original size, as measured by the cross-sectional area (Figure 5C). Pucks without cells, having been previously equilibrated near neutral pH, de-swelled instead of swelling, because they had no mechanism to raise the pH of their surroundings. The neutralization also led to a shift in the green channel to 38.6 ± 6.8 for pucks with cells (Figure 5D). The cycling of pH, swelling state, and color intensity were observed for one full cycle (representative images shown in Figure 5E). Notably, the medium surrounding gels containing cells became turbid regardless of the medium conditions, suggesting that cells were able to escape encapsulation. Fresh cell-free medium was supplemented at the start of each half cycle, further confirming that the gel serves as a reservoir for bacteria to repopulate the medium during each half cycle (Figure S8).

pH-responsive display configuration

After validating the concept of cell-driven size and color change for individual hydrogel pucks, we were interested in arranging several of them in a visual display to explore their longevity. We noticed that cell encapsulation decreased the vibrancy of color in the gels (Figure 5E). We suspected that this was due to light scattering from the cells. We confirmed the scattering effect by encapsulating 1-μm (in diameter) polystyrene beads in the hydrogel system, which led to a similar decrease in color intensity (Figure S10). To address these points, we redesigned our system to separate the cells from the color and size-changing elements. We tried several

Please cite this article in press as: Kuang et al., Microbially driven reversible size- and color-changing materials, Matter (2024), https://doi.org/10.1016/j.matt.2024.03.009

designs including some with interlinked responsive and non-responsive gels (Figure S11). However, many of these led to out-of-plane hydrogel deformations that complicated size quantification. Therefore, we opted for a design consisting of seven cell-free MR-2-containing hydrogels within a "comb" structure composed of *E. coli* encapsulated in a polyacrylamide hydrogel (Figure 6A). Because the molded hydrogel omits the acrylate monomer it is not pH responsive. This material configuration was subjected to conditions analogous to those used for individual pucks. The grouped pucks exhibited robust size and color change performance over three full cycles of acidification and neutralization (Figures 6B–6D). The endpoint pH and cell density readings for each half cycle are reported in (Figure S12).

Conclusions

Our ELM relied on the central metabolism of *E. coli* to modulate the pH, demonstrating the concept of cell reversible size and color changes driven by active metabolic processes. This is distinct from previous examples of size/shape changing ELMs.[12,13] Many living systems use environmental changes to trigger size and shape change.[26] Since microbes are limited in their ability to apply physical force to their material surroundings directly, we designed a system where pH acts as a mediator to drive the size and color change of MR-2 PAAcAAm pucks. This achievement required careful customization of the material design so that it was compatible with the living component in terms of optimal cellular growth, polymerization chemistry, and mass transfer properties. The pH range was prescribed by *E. coli*, where cell viability and production of metabolic byproducts were only possible within the range of pH 4.5 to pH 7.5. Therefore, the PAAcAAm material was selected for its ability to swell and de-swell within this pH range. Similarly, in our approach, the color changing mechanism necessitated a small-molecule dye that could be both tethered to the hydrogel matrix to prevent leaching and activated to change color within the same pH range.

While our initial goal was to demonstrate that cells could alter their pH surroundings while remaining fully encapsulated in the hydrogel matrix, we found it difficult to prevent cellular escape into the surrounding medium, where their growth and metabolic activity would outpace the encapsulated cells. Therefore, we defined our living system to be cell-laden hydrogels within the surrounding liquid medium. Considering this design concept, practical deployment would have to address containment of the living cells either through physical or genetic methods. Physical containment may be essential to the system because of the need for pH as a mediator, which is affected by volume, cell density, and buffering capabilities. Further engineering of the cellular material and device designs could improve performance factors, including the speed of state change, nutrient requirements, cellular stability, and reliability.

Previous studies have demonstrated a range of applications of pH-responsive hydrogels spanning soft robotics, actuation systems, sensors, tissue engineering, and drug delivery.[27–30] Introducing microbes, known for their diverse sensing capabilities, expands the potential input-output functions of these materials.[7,31] Furthermore, these hybrid living systems enable the development of sensing systems and devices that may reduce or eliminate the dependency to external power supplies, since microbes only require biochemical fuel to function. Future work will explore more active roles for engineered microbes to contribute to such complex functions in our platform.

For now, we demonstrate a living material in which bacteria drive reversible changes in pH to alter the size and color of the MR-2 PAAcAAm hydrogels. While these changes driven by *E. coli* rely on the native metabolism, future iterations of this

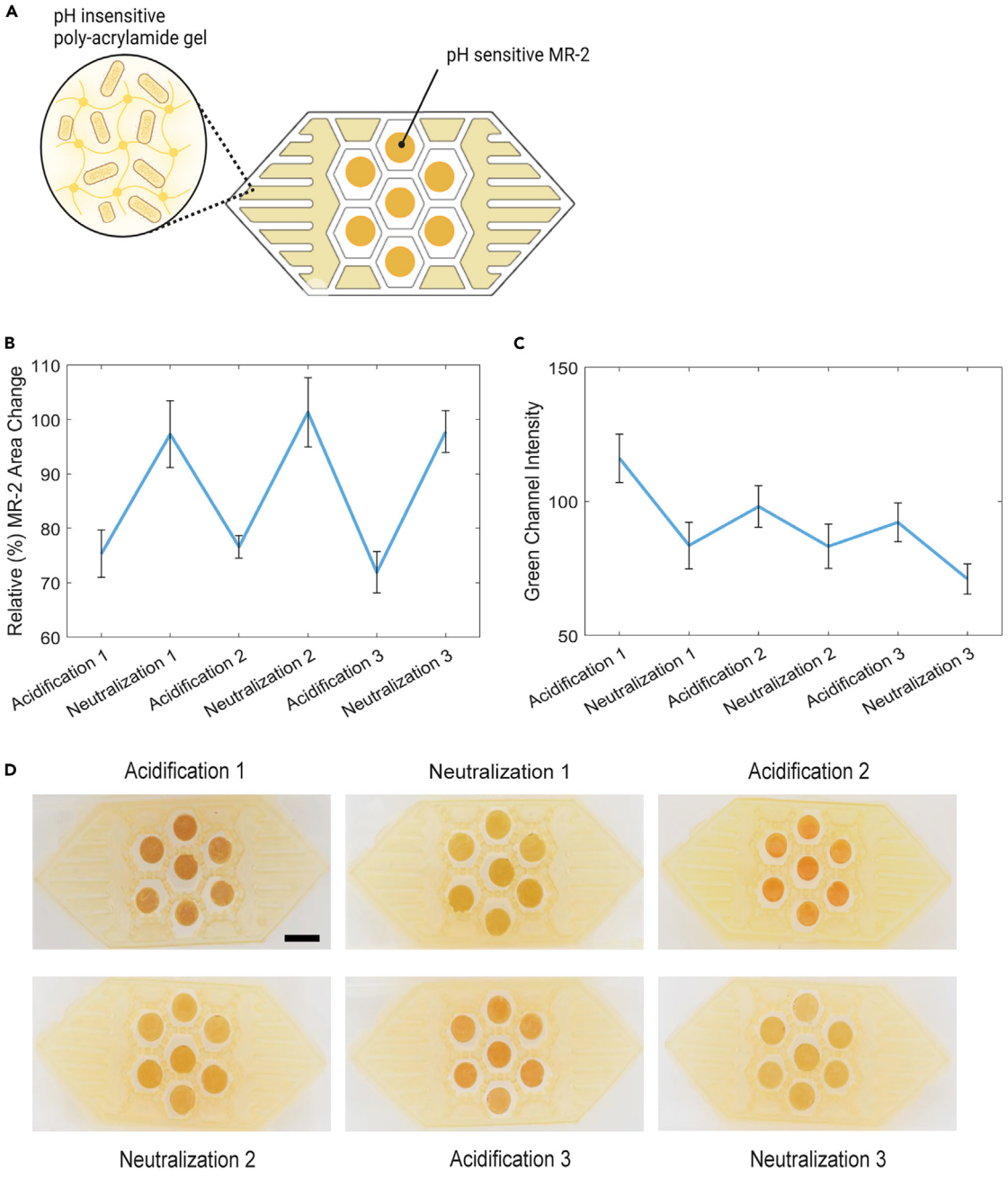

Figure 6. Cell-driven pH change in a system with cells separated from the color- and size-changing element

(A) ELM design schematic where cells are embedded in the inert polyacrylamide matrix separated from the pH-responsive hydrogel network containing MR-2.

(B) Hydrogel puck cross-sectional area measurements at the endpoint of each half cycle, where 100% represents the hydrogel puck area after initial equilibration in pH 7.5 growth medium.

(C) Green channel color intensity values of hydrogel pucks at the endpoint of each half cycle.

(D) Endpoint images representative of hydrogel puck size and color change over three full cycles.

Data in (B) and (C) are represented as mean ± SD (n = 7). Statistical tests for (B) and (C) are plotted in Figure S13.

ELM could implement genetic control over acidification and neutralization. Introducing a living driving force could allow for more complex input-output functions than currently exist for such materials.

Please cite this article in press as: Kuang et al., Microbially driven reversible size- and color-changing materials, Matter (2024), https://doi.org/10.1016/j.matt.2024.03.009

EXPERIMENTAL PROCEDURES

Resource availability

Lead contact

Further information and requests for resources and reagents should be directed to and will be fulfilled by the lead contact, Néel Joshi (ne.joshi@northeastern.edu).

Materials availability

All unique/stable reagents generated in this study are available from the lead contact with a completed materials transfer agreement.

Data and code availability

- All data reported in this paper will be shared by the lead contact upon request.
- This paper does not report original code.
- Any additional information required to reanalyze the data reported in this paper is available from the lead contact upon request.

MR-2 synthesis

O-Amino benzoic acid (1.047 g, 7.5 mM) was added to 1:1 THF/H_2O (20/20 mL) and $NaNO_2$ (0.5261 g, 7.6 mM). The mixture was stirred at 0°C continuously, while HCl (1.0 mL, 12 M) was slowly added. The resulting solution was added dropwise to a 100 mL single-neck round-bottom flask containing 1-phenylpiperazine (7.6 mM) in 1:1 THF:H_2O (40 mL), and stored at 0°C for approximately 2 h. Next, the solution was stirred overnight at room temperature. The solvent was evaporated and redissolved into $CHCl_2$ (60 mL) and washed twice with water (30 mL). The organic phase was dried over $MgSO_4$ and removed by evaporation. The crude product was purified by recrystallization using methanol, to produce MR-1 with 40% yield as a bright yellow solid. ^{1}H NMR (500 MHz, $CDCl_3$) δ 13.71 (s, 1H), 8.31 (dd, *J* = 7.9, 1.6 Hz, 1H, H-6 benzoic acid), 7.76 (dd, *J* = 8.3, 1.2 Hz, 1H, H-3 benzoic acid), 7.56 (ddd, *J* = 8.3, 7.2, 1.6 Hz, 1H, H-4 benzoic acid), 7.42–7.31 (m, 3H, H-5 benzoic acid, H-2 Ph, H-6 Ph), 7.09–6.91 (m, 2H, H-3 Ph, H-5 Ph), 4.11 (dt, *J* = 82.9, 5.5 Hz, 4H, piperazine), 3.67–3.42 (m, 4H, piperazine). ^{13}C NMR (126 MHz, $CDCl_3$) δ 167.24, 150.04, 148.02, 133.65, 132.65, 129.48, 126.81, 122.23, 121.06, 116.78, 116.01, 52.06, 49.81, 47.47, 44.78; HRMS (ESI) Calcd for $[M + H]^+$ $C_{17}H_{18}N_4O_2$: 311.1430. Found 311.1498.

Next, MR-1 (0.5 g, 1.6 mM) was dissolved in CH_2Cl_2 (8 mL) and stirred at 0°C. The solution was slowly added to a mixture of Et_3N (0.3 mL, 2.5 mM) and acryloyl chloride (0.327 g, 1.93 mM) dropwise, and left stirring overnight at room temperature. The resulting dark red solution was evaporated, redissolved into $CHCl_2$ (60 mL), and washed twice with water (30 mL). The organic phase was dried over $MgSO_4$ and removed by evaporation. The crude product was purified on a silica column using 70:30 Hex:EtOAc, to produce MR-2 with 60% yield as a bright red solid. ^{1}H NMR (500 MHz, $CDCl_3$) δ 8.11 (d, *J* = 7.6 Hz, 1H, benzoic acid), 7.48 (t, *J* = 7.6 Hz, 1H, benzoic acid), 7.34–7.26 (m, 3H, benzoic acid, Ph), 6.93 (dd, *J* = 15.4, 7.7 Hz, 3H, Ph), 6.62 (dd, *J* = 16.8, 10.5 Hz, 1H, acryloyl CHC$\underline{H}_2$), 6.35 (dd, *J* = 16.8, 1.8 Hz, 1H, acryloyl CHC$\underline{H}_2$), 5.75 (dd, *J* = 10.5, 1.8 Hz, 1H, acryloyl C$\underline{H}$CH$_2$), 3.81 (dt, *J* = 66.3, 5.0 Hz, 4H, piperazine), 3.26–3.11 (m, 4H, piperazine). ^{13}C NMR (126 MHz, $CDCl_3$) δ 165.54, 150.87, 133.54, 130.14, 129.28, 128.46, 128.32, 127.28, 120.67, 116.72, 111.66, 49.89, 49.39, 45.77, 41.94.; HRMS (ESI) Calcd for $[M + H]^+$ $C_{20}H_{21}N_4O_3$: 365.1608. Found 365.1602.

Cell strains and plasmids

E. coli (BL21) (Thermo Scientific) was transformed with appropriate plasmid variants, empty pET21d(+) ("sham") (EMD Millipore) or pSecGFP[32] for experiments. The sham

Please cite this article in press as: Kuang et al., Microbially driven reversible size- and color-changing materials, Matter (2024), https://doi.org/10.1016/j.matt.2024.03.009

plasmid contains an ampicillin resistance gene and a T7 expression system, which does not contain coding genes. The pSecGFP plasmid contains a kanamycin resistance gene and PLlacO-1 (LacI regulated) promoter encoding cytosolic superfolder GFP (sfGFP).

Cell culture

E. coli bacteria were grown in LB broth, which was prepared as follows: 10 g of tryptone, 5 g of yeast extract, and 10 g of NaCl, dissolved in 1 L of dH_2O. For all experiments, starter cultures of the appropriate transformed strain were grown overnight in LB medium in a shaking incubator (Infors HT) at 37°C and 225 RPM. All BL21 sham cultures were supplemented with carbenicillin (100 μg/mL), and BL21 pSecGFP cultures were supplemented with kanamycin (50 μg/mL). All cell cultivation and hydrogel cycling experiments containing cells were incubated at 37°C in a shaking incubator at 225 rpm overnight unless otherwise noted.

MR-2 PAAcAAm fabrication

PAAcAAm hydrogels were prepared using the molar ratios of precursor gel components shown in Table 1. In brief, MR-2 (40 μL, 1 mg/μL acrylic acid), acrylamide (50 mg, RPI, cat. no. A11260), bis-acrylamide (6 mg, RPI, cat. no. A11270), and acrylic acid (7.4 μL, Fisher Scientific cat. no. AC164252500) were combined with dH_2O (up to 4 mL) and vortexed until homogenized. Using a pH probe (Thermo Scientific, STARA2218), the pH of the solution was monitored and adjusted with concentrated sodium hydroxide until the solution reached pH 8.0, then adjusted to 4.2 mL with dH_2O. In instances where cells were encapsulated in hydrogels, cultures were normalized to OD_{600} = 2.0 before cell pelleting by centrifugation (Beckman Coulter) at 4,000 × *g* for 10 min at 4°C. The cell pellets were then resuspended in the precursor solution to a density of 2.3×10^{10} per mL of the precursor solution. A 10% (w/v) concentration of ammonium persulfate (APS) (160 μL/mL of precursor solution, Fisher Scientific, cat. no. BP179-25), and *N*,*N*,*N*′,*N*′-tetramethylethylenediamine (TEMED, 4 μL/mL of precursor solution, Thermo Fisher Scientific, cat. no. J63734.AC) were added to the solution followed by vortexing. Next, 60 μL of the solution was aliquoted into each well of a 3D-printed elastic 50A resin (Formlabs) mold to form cylindrical hydrogel (pucks). The pucks polymerized for 1 h at room temperature and were 6 mm in diameter and 2.12 mm in height directly after removal from the molds.

Area image analysis

Images were imported into ImageJ and color thresholded to isolate the hydrogel pucks. Using the analyze particles command, the area in mm^2 was calculated for each puck, then converted to relative percent change in area compared with the equilibration endpoint for each individual puck. Data are reported as mean and standard deviation in relative percent area change.

Color image analysis

Images were imported into ImageJ and then separated into RGB color channels. In the green channel, the mean thresholded color intensity was taken for each puck. The mean of these values across pucks was normalized by subtracting from pure white (255). These normalized values were graphed with positive and negative errors equal to the standard deviation. Images in Figures 5 and 6 were adjusted using Photoshop to normalize brightness intensities.

MR-2 loading density in cell-free hydrogels

Cell-free MR-2 hydrogel pucks were prepared as described in the MR-2 PAAcAAm fabrication methods, but MR-2 concentration was varied as follows: 0%, 1.7%,

Please cite this article in press as: Kuang et al., Microbially driven reversible size- and color-changing materials, Matter (2024), https://doi.org/10.1016/j.matt.2024.03.009

3.3%, and 6.7% (w/v). Polymerized pucks for each MR-2 loading density were immersed in 5 mL of sodium citrate buffer at pH 4.0 (n = 3) or 5 mL of Tris-HCl buffer at pH 7.0 (n = 3). After 24 h, MR-2 pucks were removed from the buffers and photographed for analysis of size and color in ImageJ, as described in the area image analysis and color image analysis methods, respectively. The 6.7% loading density of MR-2 was used for all other experiments.

pH equilibrium for cell-free hydrogels

Sample populations of MR-2 hydrogel pucks (n = 3) were immersed in aqueous solutions buffered to a pH range of 4.0–8.0. The pH 4.0–6.0 buffers were sodium citrate and the pH 7.0–8.0 buffers were Tris-HCl. After 24 h of equilibration in the various buffers, pucks were photographed for analysis of size and color in ImageJ, as described in the area image analysis and color image analysis methods, respectively.

pH cycling experiments for cell-free hydrogels

Immediately after polymerization, MR-2 hydrogel pucks were equilibrated in 5 mL of Tris-HCl buffer at pH 7.0 for 20 h. Next, the pucks were transferred to 5 mL of fresh sodium citrate buffer at pH 4.0 for 24 h to complete the acidification half cycle. Following this, the pucks were transferred to 5 mL of fresh Tris-HCl buffer at pH 7.0 for 24 h to complete the neutralization half cycle. Each half cycle makes one full cycle, and cycling was continued over two full cycles. Photos of the hydrogel pucks were taken at the endpoints of equilibration, acidification, and neutralization. Photos were analyzed following the area image analysis and color image analysis methods.

Perfusion chamber construction

A custom fluidic system was used to perform automated exchanges of acidic and neutral buffers to drive size and color changes in our gels. The fluid control system comprised two liquid reservoir bottles (500 mL) connected to an enclosed device containing pucks using a central fluidic union. The tubing between each reservoir and the device was interrupted by a solenoid valve that was turned on and off by signals from a microcontroller (Arduino). The reservoirs were positioned above the device containing the gels and vented to atmospheric pressure, so that when one of the solenoid valves was opened, fluid was driven into the gel chamber by gravity. By opening and closing the solenoid valves corresponding to acidic and neutral buffers in a timed sequence programmed onto the microcontroller, controlled gravity flow was used to automate long-term fluid exchange experiments.

The fluidic chamber was prepared from a combination of laser-cut acrylic sheets and silicone gaskets. The bottom layer, through which the gels were imaged via time-lapse imaging (Epson v.39 photo scanner) was made with 1/8-inch-thick acrylic and contained threaded holes (no. 6-32) around the perimeter, which were used to fasten the layers of the device together. Through-holes at these positions were incorporated into all other layers so that the device could be assembled by stacking components from the bottom up. The second layer of the device was prepared from fiber-reinforced silicone rubber (McMaster-Carr), with a large hexagonal cutout matching the geometry of the fluidic chamber cut into the acrylic layer above. This third layer was prepared from 1/4-inch-thick acrylic and featured a hexagonal cutout that created the volume in which gel pucks were held for cycling and imaging. The volume of this chamber was approximately 20 mL. We designed a 3D-printed hexagonal insert for this chamber, which featured smaller hexagonal geometries, just large enough to hold fully expanded gel pucks in an arrayed pattern during our experiments. A fourth layer, identical to the second layer, was prepared from

Please cite this article in press as: Kuang et al., Microbially driven reversible size- and color-changing materials, Matter (2024), https://doi.org/10.1016/j.matt.2024.03.009

fiber-reinforced silicone to seal the fluidic chamber of the device. The fifth and final layer was a continuous piece of white 1/4-inch-thick acrylic that sealed over the hexagonal chamber, closing the system. This layer featured two threaded holes for Luer lock connectors at either end of the hexagonal chamber, which was connected to the microcontroller-based system described above on one side and an outlet to a waste bottle on the other side. During each buffer exchange cycle, fresh buffer entered the device from one side and evacuated the existing fluid in the chamber to waste. Representative images of the fluidic control system and perfusion chamber are shown in (Figure S5).

Perfusion chamber cycling experiments

To demonstrate the long-term reproducibility of hydrogel size and color change, we programmed the microcontroller of our fluidic system to execute 24-h cycles featuring a 12-h half cycle of acidic (pH 4.0) buffer, followed by a 12-h half cycle of neutral (pH 7.0 buffer). In these experiments, we found that gel cycling was improved by performing an additional automated exchange 4 h into each acidic half cycle to aid in the gel de-swelling process. We allowed these continuous experiments to run for up to 400 h and collected time-lapse images to measure gel size and color intensity.

BacTiter-Glo Cell Viability Assay

Cell-embedded MR-2 PAAcAAm pucks were prepared as described in the MR-2 PAAcAAm fabrication methods but with varied volumes of BL21 sham culture at OD_{600} = 2.0/mL (2.3 × 10^{10} CFU/mL), which was cell pelleted and resuspended in 1 mL of precursor solution. The varied volumes ranged from 0 to 100 mL of cell culture. After polymerization, pucks (n = 3) for each cell density condition underwent the BacTiter-Glo Microbial Cell Viability Assay (Promega), as described in the manufacturer's instruction manual. An additional sample group (n = 3) for each cell density was equilibrated overnight in PBS at room temperature before performing the viability assay on day 2.

Confocal microscopy

After fabrication, PAAcAAm gel pucks containing *E. coli* pSec-GFP were stored in 1× PBS at 4°C for 16 h, then imaged using laser scanning confocal microscopy. The gels were bisected into horizontal cross-sections using a razor and placed on a no. 1.0 glass coverslip (Fisher Scientific) for z stack scanning. Stacks were imaged at random placements near the center of the gels. Imaging was performed using a Zeiss LSM 800 inverted laser-scanning confocal microscope with a Zeiss Plan-Achromat Korr sM27 objective lens (40×, numerical aperture 0.95). Data were gathered using a laser excitation wavelength of 488 nm and detection wavelengths ranging from 400 to 624 nm with a GaAsP-PMT detector in frame-scan mode (1.27 s/frame). The pixel scaling was set to 0.156 × 0.156 μm, with vertical z spacing of 1.000 μm. The pinhole of the confocal was set to 0.55 AU/24 μm. Frame size was set to 159.73 × 159.73 μm, and z stacks of roughly 125 slices (124 μm total) were obtained. Data were visualized using FIJI's 3D Reconstruction/Volume Rendering plugin.

GFP expression viability assay

MR-2 PAAcAAm gel pucks containing BL21 sham or pSec-GFP plasmid were incubated overnight in LB medium containing appropriate antibiotics. Following overnight equilibration, medium was replaced with fresh LB broth, antibiotics, and 10 μM IPTG, if necessary, for induction. The pucks were incubated overnight and then imaged under bright-field and Alexa Fluor 546 using the ChemiDoc MP System.

Please cite this article in press as: Kuang et al., Microbially driven reversible size- and color-changing materials, Matter (2024), https://doi.org/10.1016/j.matt.2024.03.009

Mean gray value analysis

Eight-bit images from GFP expression assay taken using the ChemiDoc were imported into ImageJ. The average gray value was calculated for each individual puck by selecting the region of interest and measuring the area using the mean gray value option. The average and standard deviations for each condition were plotted.

pH cycling of free cells in suspension culture

BL21 sham cultures were normalized to OD_{600} = 1.5, and 10 mL of normalized culture was pelleted by centrifugation at 4,000 × *g* for 10 min at 4°C. Cell pellets were resuspended in 10 mL of acidification cycle medium (LB medium with 2% glucose and appropriate antibiotics at pH 7.5; n = 3), or neutralization cycle medium (LB medium with 1 mM acetate and appropriate antibiotics at pH 4.5; n = 3). Cultures were incubated for 18 h, before measuring the pH and OD_{600} of the suspension culture.

pH cycling experiments for cell-embedded hydrogels

Immediately after polymerization, cell-embedded MR-2 hydrogel pucks were equilibrated in a 12-well plate with one puck per well and 2 mL of LB medium (per well) at pH 7.5. After collecting endpoints, the medium was aspirated from the wells, followed by the addition of 2 mL of LB medium with 2% glucose at pH 7.5 for the acidification half cycle. After 20 h of incubation, the medium was aspirated and replaced with 2 mL of LB medium with 1 mM acetate at pH 4.5 for the neutralization half cycle, which was also conducted over 20 h of incubation. The pH of the suspension at the end of equilibration and each half cycle was measured using a pH probe. Furthermore, photos of hydrogel pucks were taken at each endpoint for analysis of area and color in ImageJ, and OD_{600} of the suspension medium was measured at each endpoint using a SpectraMax M5 plate reader. Appropriate antibiotics were provided in the medium throughout the course of the experiment.

Polystyrene nanoparticle light scattering experiment

Polystyrene nanoparticles were encapsulated in MR-2 PAAcAAm hydrogel pucks following the same precursor preparation steps as outlined in the MR-2 PAAcAAm fabrication methods. After mixing precursor reagents and adjusting the pH to 8.0, 1 μm polystyrene beads was added to the precursor at a volume matching the converted volume of *E. coli* encapsulated in PAAcAAm precursor based on CFU as described in MR-2 PAAcAAm fabrication. The solution was vortexed to distribute the beads. Then, APS and TEMED were added at appropriate concentrations before vortexing and aliquoting into the resin mold. After polymerization, pucks (n = 3) were equilibrated and then cycled as described in the pH cycling experiments for cell-free hydrogels methods for one full cycle.

Two-phase system fabrication

BL21 sham cultures were normalized to OD_{600} = 2.0 and cell pelleted by centrifugation at 4,000 × *g* for 10 min at 4°C. The cell pellet was resuspended in acrylamide solution (1.4 M) to achieve a density of 2.3×10^{10} CFU per mL of precursor solution. Next, 10% (w/v) APS (160 μL/mL of precursor solution) and TEMED (4 μL/mL of precursor solution) were added to the solution, which was then vortexed and pipetted into specific chambers of a 3D-printed elastic 50A resin (Formlabs) mold as shown in Figure 6A. The mold was incubated for 20 min at room temperature to allow polymerization to reach completion.

Two-phase system cycling

Seven MR-2 (cell-free) hydrogel pucks were placed individually in the open chambers of the 3D-printed resin mold containing fully polymerized cell-embedded

polyacrylamide. The entire system containing cell-embedded polyacrylamide and pH-responsive MR-2 pucks was equilibrated overnight and immersed with pH 7.5 LB medium (30 mL) in a single-well plate for 18 h. After equilibration, endpoint pH and OD_{600} readings were measured from the suspension medium. The photos were acquired using a Canon EOS Rebel SL3 camera for size and color analysis of MR-2 pucks in ImageJ. Next, the remaining suspension medium was aspirated and replaced with LB medium containing 2% glucose at pH 7.5 to conduct the acidification cycle overnight for 18 h. After acquiring endpoint pH, OD_{600}, and photos for the acidification cycle, the medium was removed and replaced with LB medium containing 1 mM acetate at pH 4.5 to conduct the neutralization cycle overnight for 18 h. The experiment was continued for three full cycles collecting endpoints after each acidification and neutralization cycle. Appropriate antibiotics were provided in the medium throughout the course of the experiment.

SUPPLEMENTAL INFORMATION

Supplemental information can be found online at https://doi.org/10.1016/j.matt.2024.03.009.

ACKNOWLEDGMENTS

J.K. and S.B. contributed equally to this work. This work was supported by the Government of the United States under a Partnership Intermediary Agreement. The US Government is authorized to reproduce and distribute reprints for Government purposes notwithstanding any copyright notation thereon. The views and conclusions contained herein are those of the authors and should not be interpreted as necessarily representing the official policies or endorsements, either expressed or implied, of the US Government. This work was also supported by the National Science Foundation (DMR 2004875) and the Novo Nordisk Foundation Challenge Programme 2022 – Energy Materials with Biological Applications grant no. NNF22OC0071130. We thank the Institute for Chemical Imaging of Living Systems at Northeastern University for consultation and imaging support. Graphics were created with BioRender.com.

AUTHOR CONTRIBUTIONS

Conceptualization, J.K., S.B., D.J.W., L.F.D., and N.S.J.; methodology, J.K., S.B., W.-T.C., and D.Q.B.; validation, J.K., S.B., and W.-T.C.; formal analysis, J.K., S.B., W.-T.C., D.Q.B., V.M.P., J.Z., N.S., L.A.Y., and O.J.A.; investigation, D.J.W., L.F.D., and N.S.J.; data curation, J.K., S.B., W.-T.C., D.Q.B., V.M.P., J.Z., N.S., L.A.Y., O.J.A., M.H.A., and S.L.L.; writing – original draft, J.K., S.B., and W.-T.C.; writing – review & editing, J.K., S.B., D.J.W., L.F.D., and N.S.J.; visualization, J.K., S.B., W.-T.C., V.M.P., J.Z., N.S., and O.J.A.; supervision, D.J.W., L.F.D., and N.S.J.; project administration, D.J.W., L.F.D., and N.S.J.; funding acquisition, D.J.W., L.F.D., and N.S.J.

DECLARATION OF INTERESTS

The authors are inventors on a US Provisional Patent Application (63/383,698) submitted by Northeastern University.

Received: October 24, 2023
Revised: January 4, 2024
Accepted: March 20, 2024
Published: April 11, 2024

REFERENCES

1. Nakamura, S., and Minamino, T. (2019). Flagella-Driven Motility of Bacteria. Biomolecules *9*, 279. https://doi.org/10.3390/biom9070279.

2. Hofhuis, H., Moulton, D., Lessinnes, T., Routier-Kierzkowska, A.-L., Bomphrey, R.J., Mosca, G., Reinhardt, H., Sarchet, P., Gan, X., Tsiantis, M., et al. (2016). Morphomechanical Innovation Drives Explosive Seed Dispersal. Cell *166*, 222–233. https://doi.org/10.1016/j.cell.2016.05.002.

3. (2018). Muscles and Skeletons: The Building Blocks of Animal Movement. In Animal Locomotion, A. Biewener, S. Patek, A.A. Biewener, and S.N. Patek, eds. (Oxford University Press). https://doi.org/10.1093/oso/9780198743156.003.0002.

4. Grébert, T., Doré, H., Partensky, F., Farrant, G.K., Boss, E.S., Picheral, M., Guidi, L., Pesant, S., Scanlan, D.J., Wincker, P., et al. (2018). Light color acclimation is a key process in the global ocean distribution of Synechococcus cyanobacteria. Proc. Natl. Acad. Sci. *115*, E2010–E2019. https://doi.org/10.1073/pnas.1717069115.

5. Archetti, M., Döring, T.F., Hagen, S.B., Hughes, N.M., Leather, S.R., Lee, D.W., Lev-Yadun, S., Manetas, Y., Ougham, H.J., Schaberg, P.G., and Thomas, H. (2009). Unravelling the evolution of autumn colours: an interdisciplinary approach. Trends Ecol. Evol. *24*, 166–173. https://doi.org/10.1016/j.tree.2008.10.006.

6. Mäthger, L.M., Denton, E.J., Marshall, N.J., and Hanlon, R.T. (2009). Mechanisms and behavioural functions of structural coloration in cephalopods. J. R. Soc. Interface *6*, S149–S163. https://doi.org/10.1098/rsif.2008.0366.focus.

7. Liu, X., Tang, T.-C., Tham, E., Yuk, H., Lin, S., Lu, T.K., and Zhao, X. (2017). Stretchable living materials and devices with hydrogel–elastomer hybrids hosting programmed cells. Proc. Natl. Acad. Sci. *114*, 2200–2205. https://doi.org/10.1073/pnas.1618307114.

8. Mimee, M., Nadeau, P., Hayward, A., Carim, S., Flanagan, S., Jerger, L., Collins, J., McDonnell, S., Swartwout, R., Citorik, R.J., et al. (2018). An ingestible bacterial-electronic system to monitor gastrointestinal health. Science *360*, 915–918. https://doi.org/10.1126/science.aas9315.

9. Gilbert, C., Tang, T.-C., Ott, W., Dorr, B.A., Shaw, W.M., Sun, G.L., Lu, T.K., and Ellis, T. (2021). Living materials with programmable functionalities grown from engineered microbial co-cultures. Nat. Mater. *20*, 691–700. https://doi.org/10.1038/s41563-020-00857-5.

10. Liang, L., Heveran, C., Liu, R., Gill, R.T., Nagarajan, A., Cameron, J., Hubler, M., Srubar, W.V., and Cook, S.M. (2018). Rational Control of Calcium Carbonate Precipitation by Engineered Escherichia coli. ACS Synth. Biol. *7*, 2497–2506. https://doi.org/10.1021/acssynbio.8b00194.

11. Greca, L.G., Lehtonen, J., Tardy, B.L., Guo, J., and Rojas, O.J. (2018). Biofabrication of multifunctional nanocellulosic 3D structures: a facile and customizable route. Mater. Horiz. *5*, 408–415. https://doi.org/10.1039/C7MH01139C.

12. Rivera-Tarazona, L.K., Bhat, V.D., Kim, H., Campbell, Z.T., and Ware, T.H. (2020). Shape-morphing living composites. Sci. Adv. *6*, eaax8582. https://doi.org/10.1126/sciadv.aax8582.

13. Wang, W., Yao, L., Cheng, C.-Y., Zhang, T., Atsumi, H., Wang, L., Wang, G., Anilionyte, O., Steiner, H., Ou, J., et al. (2017). Harnessing the hygroscopic and biofluorescent behaviors of genetically tractable microbial cells to design biohybrid wearables. Sci. Adv. *3*, e1601984. https://doi.org/10.1126/sciadv.1601984.

14. Nawroth, J.C., Lee, H., Feinberg, A.W., Ripplinger, C.M., McCain, M.L., Grosberg, A., Dabiri, J.O., and Parker, K.K. (2012). A tissue-engineered jellyfish with biomimetic propulsion. Nat. Biotechnol. *30*, 792–797. https://doi.org/10.1038/nbt.2269.

15. Liu, X., Gao, M., Chen, J., Guo, S., Zhu, W., Bai, L., Zhai, W., Du, H., Wu, H., Yan, C., et al. (2022). Recent Advances in Stimuli-Responsive Shape-Morphing Hydrogels. Adv. Funct. Mater. *32*, 2203323. https://doi.org/10.1002/adfm.202203323.

16. Francis, N.L., Hunger, P.M., Donius, A.E., Riblett, B.W., Zavaliangos, A., Wegst, U.G.K., and Wheatley, M.A. (2013). An ice-templated, linearly aligned chitosan-alginate scaffold for neural tissue engineering. J. Biomed. Mater. Res. *101*, 3493–3503. https://doi.org/10.1002/jbm.a.34668.

17. Qu, J., Zhao, X., Ma, P.X., and Guo, B. (2017). pH-responsive self-healing injectable hydrogel based on N-carboxyethyl chitosan for hepatocellular carcinoma therapy. Acta Biomater. *58*, 168–180. https://doi.org/10.1016/j.actbio.2017.06.001.

18. Williamson, P., Ijäs, H., Shen, B., Corrigan, D.K., and Linko, V. (2021). Probing the Conformational States of a pH-Sensitive DNA Origami Zipper via Label-Free Electrochemical Methods. Langmuir *37*, 7801–7809. https://doi.org/10.1021/acs.langmuir.1c01110.

19. Yang, C., Su, F., Liang, Y., Xu, W., Li, S., Liang, E., Wang, G., Zhou, N., Wan, Q., and Ma, X. (2020). Fabrication of a biomimetic hydrogel actuator with rhythmic deformation driven by a pH oscillator. Soft Matter *16*, 2928–2932. https://doi.org/10.1039/C9SM02519G.

20. Bhusari, S., Kim, J., Polizzi, K., Sankaran, S., and del Campo, A. (2023). Encapsulation of bacteria in bilayer Pluronic thin film hydrogels: A safe format for engineered living materials. Biomater. Adv. *145*, 213240. https://doi.org/10.1016/j.bioadv.2022.213240.

21. Liu, X., Inda, M.E., Lai, Y., Lu, T.K., and Zhao, X. (2022). Engineered Living Hydrogels. Adv. Mater. *34*, 2201326. https://doi.org/10.1002/adma.202201326.

22. Reed, J.L., Vo, T.D., Schilling, C.H., and Palsson, B.O. (2003). An expanded genome-scale model of Escherichia coli K-12 (iJR904 GSM/GPR). Genome Biol. *4*, R54. https://doi.org/10.1186/gb-2003-4-9-r54.

23. Srinivasan, K., and Mahadevan, R. (2010). Characterization of proton production and consumption associated with microbial metabolism. BMC Biotechnol. *10*, 2. https://doi.org/10.1186/1472-6750-10-2.

24. Humans, I.W.G. on the E. of C.R. to (2010). GENERAL INTRODUCTION TO THE CHEMISTRY OF DYES. In Some Aromatic Amines, Organic Dyes, and Related Exposures. (International Agency for Research on Cancer).

25. Zhao, N., Catrysse, P.B., and Fan, S. (2021). Perfect RGB-IR Color Routers for Sub-Wavelength Size CMOS Image Sensor Pixels. Adv. Photonics Res. *2*, 2000048. https://doi.org/10.1002/adpr.202000048.

26. Le Duigou, A., and Castro, M. (2016). Evaluation of force generation mechanisms in natural, passive hydraulic actuators. Sci. Rep. *6*, 18105. https://doi.org/10.1038/srep18105.

27. Shojaeifard, M., Bayat, M.R., and Baghani, M. (2019). Swelling-induced finite bending of functionally graded pH-responsive hydrogels: a semi-analytical method. Appl. Math. Mech. *40*, 679–694. https://doi.org/10.1007/s10483-019-2478-6.

28. Houben, S.J.A., Lugger, S.J.D., van Raak, R.J.H., and Schenning, A.P.H.J. (2022). A pH-Responsive Liquid Crystal Hydrogel Actuator with Calcium-Induced Reprogrammable Shape Fixing. ACS Appl. Polym. Mater. *4*, 1298–1304. https://doi.org/10.1021/acsapm.1c01686.

29. Jiang, S., Xia, L., Ma, H., Yang, T., and Qian, L. (2023). pH and temperature dual-responsive hydrogel actuator with bidirectional bending behavior and ultra large bending angle. Eur. Polym. J. *197*, 112296. https://doi.org/10.1016/j.eurpolymj.2023.112296.

30. Jiang, H., Yu, W., Zhou, J., and Ziaie, B. (2017). A pH-sensitive hydrogel-based smart switch for GI-tract payload release. In 2017 IEEE 30th International Conference on Micro Electro Mechanical Systems (MEMS), pp. 510–513. https://doi.org/10.1109/MEMSYS.2017.7863455.

31. Pardee, K., Green, A.A., Ferrante, T., Cameron, D.E., DaleyKeyser, A., Yin, P., and Collins, J.J. (2014). Paper-based synthetic gene networks. Cell *159*, 940–954. https://doi.org/10.1016/j.cell.2014.10.004.

32. Emani, S.S., Kan, A., Storms, T., Bonanno, S., Law, J., Ray, S., and Joshi, N.S. (2023). Periplasmic stress contributes to a tradeoff between protein secretion and cell growth in Escherichia coli Nissle 1917. Synth. Biol. *8*, ysad013. https://doi.org/10.1093/synbio/ysad013.